

Journal of Biomedical Optics

SPIEDigitalLibrary.org/jbo

Preclinical study of using multiphoton microscopy to diagnose liver cancer and differentiate benign and malignant liver lesions

Jun Yan
Shuangmu Zhuo
Gang Chen
Xiufeng Wu
Dong Zhou
Shusen Xie
Jiahao Jiang
Mingang Ying
Fan Jia
Jianxin Chen
Jian Zhou

Preclinical study of using multiphoton microscopy to diagnose liver cancer and differentiate benign and malignant liver lesions

Jun Yan,^{a,c,*} Shuangmu Zhuo,^{b,*} Gang Chen,^{d,*} Xiufeng Wu,^c Dong Zhou,^c Shusen Xie,^b Jiahao Jiang,^a Mingang Ying,^c Fan Jia,^a Jianxin Chen,^b and Jian Zhou^a

^aFudan University, Zhongshan Hospital, Liver Cancer Institute, Shanghai 200032, China

^bFujian Normal University, Institute of Laser and Optoelectronics Technology, Fujian Provincial Key Laboratory for Photonics Technology, Key Laboratory of Optoelectronic Science and Technology for Medicine of Ministry of Education, Fuzhou 350007, China

^cTeaching Hospital of Fujian Medical University, Fujian Provincial Tumor Hospital, Department of Surgery, Fuzhou 350014, China

^dTeaching Hospital of Fujian Medical University, Fujian Provincial Tumor Hospital, Department of Pathology, Fuzhou 350014, China

Abstract. Recently, the miniaturized multiphoton microscopy (MPM) and multiphoton probe allow the clinical use of multiphoton endoscopy for diagnosing cancer via “optical biopsy”. The purpose of this study was to establish MPM optical diagnostic features for liver cancer and evaluate the sensitivity, specificity, and accuracy of MPM optical diagnosis. Firstly, we performed a pilot study to establish the MPM diagnostic features by investigating 60 surgical specimens, and found that high-resolution MPM images clearly demonstrated apparent differences between benign and malignant liver lesions in terms of their tissue architecture and cell morphology. Cancer cells, characterized by irregular size and shape, enlarged nuclei, and increased nuclear-cytoplasmic ratio, were identified by MPM images, which were comparable to hematoxylin-eosin staining images. Secondly, we performed a blinded study to evaluate the sensitivity, specificity, and accuracy of MPM optical diagnosis by investigating another 164 specimens, and found that the sensitivity, specificity, and accuracy of MPM diagnosis was 96.32%, 96.43%, and 96.34%, respectively. In conclusion, it is feasible to use MPM to diagnose liver cancer and differentiate benign and malignant liver lesions. This preclinical study provides the groundwork for further using multiphoton endoscopy to perform real-time noninvasive “optical biopsy” for liver lesions in the near future.

© 2012 Society of Photo-Optical Instrumentation Engineers (SPIE). [DOI: 10.1117/1.JBO.17.2.026004]

Keywords: multiphoton microscopy; optical diagnosis; liver cancer; liver lesions; pathology.

Paper 11595 received Oct. 12, 2011; revised manuscript received Nov. 21, 2011; accepted for publication Dec. 7, 2011; published online Feb. 22, 2012.

1 Introduction

Liver biopsy turns out to be invaluable in making diagnoses, in monitoring the progression of various liver diseases, and in evaluating the effects of the therapy. Although the reasons for performing liver biopsies have slightly changed over the years, the need for doing so has not. Diagnosis of liver cancer or space-occupying lesions is a traditional application for the liver biopsy and remains useful today, especially before the liver transplantation.¹ However, there are several disadvantages of liver biopsy in clinic. Firstly, biopsy for suspicious liver lesions has risks such as bleeding, bile leak, tumor dissemination, and needle track seeding.^{2–5} Secondly, the routine histopathological diagnosis after the biopsy is time-consuming in that the specimen preparation procedure requires sample fixation, slicing and labeling, and sometimes the result is ambiguous or negative because the sample is too little or tissue necrosis may incur. Finally, tumor nodules, either deep or superficial, can be missed by the relatively blind percutaneous technique, even when performed with the aid of computed tomography.

Therefore, the availability of a noninvasive “optical biopsy” that can obtain real-time histopathologic images comparable to golden standard hematoxylin-eosin (H-E) staining images will be of extraordinary benefits to the medical community.

Multiphoton microscopy (MPM), based on the advancement of the field of non-linear optics and femtosecond lasers, can provide real-time detailed information about tissue architecture and cell morphology in live tissue using a combination of autofluorescence from cells and second harmonic generation (SHG) signal from collagen.^{6–8} Natural intrinsic fluorophores abundantly present in the most cells include reduced nicotinamide adenine dinucleotide (NADH) and flavin adenine dinucleotides (FAD).⁹ Moreover, MPM can reveal cell metabolism via NADH and FAD redox ratio without the administration of exogenous contrast agents.^{10,11} Thus, MPM has great potential to noninvasively evaluate and monitor morphological structures and the functional states of living tissues.

Recently, the miniaturized MPM and multiphoton probe allow the clinical use of multiphoton endoscopy for diagnosing cancer.^{12–20} Therefore, establishing MPM optical diagnostic features is essential and significant for developing multiphoton endoscopy to diagnose liver cancer and differentiate benign and malignant liver lesions. Until now, these MPM diagnostic features have not been clearly described. The purpose of this

*These authors contributed equally to this work.

Address all correspondence to: Jian Zhou, Fudan University, Zhongshan Hospital, Liver Cancer Institute, 180 Fenglin Road, Shanghai 200032, China. Tel: 086-21-64041990; Fax: 086-21-64037181; E-mail: zhou.jian@zs-hospital.sh.cn, or Shuangmu Zhuo, Fujian Normal University, Institute of Laser and Optoelectronics Technology, Fuzhou, Fujian 350007, China. Tel: 086 591 22686078; Fax: 086 591 83465212; E-mail: shuangmuzhuo@gmail.com.

study is to establish MPM optical diagnostic features for liver cancer and evaluate the sensitivity, specificity, and accuracy of MPM optical diagnosis. To the best of our knowledge, this is the first study to use MPM to diagnose liver cancer.

2 Materials and Methods

2.1 Study Design

There were two steps in this research. Firstly, a pilot study was performed to establish the MPM diagnostic features by investigating 60 surgical specimens between July 2009 and August 2010. Then, a blinded study was conducted to evaluate the sensitivity, specificity, and accuracy of MPM optical diagnosis by investigating another 164 specimens obtained from the liver tissues bank at the Liver Cancer Institute of Fudan University between September 2010 and July 2011. This research was approved by the Institutional Review Board. All the patients from whom tissue samples were obtained provided written informed consent.

2.2 Samples Preparation

In the pilot study, 60 fresh, unfixed, and unstained human liver lesions, including hepatocellular carcinomas, cholangiocarcinomas, metastatic tumors, focal nodular hyperplasias, adenomas, hemangiomas, and regenerative nodules in liver cirrhosis, were obtained from 60 patients who had undergone hepatectomy between July 2009 and August 2010. Each of the liver lesions, once being removed from liver, was placed in a standard pathologic transport container covered with ice and then sent to pathologic lab. For the lesions on the liver surface, each sample approximately $2 \times 1 \times 1$ cm in size from surface to inside was taken by pathologist. For the lesions in deep part of the liver, the specimens were opened to find the lesions, and each sample approximately $2 \times 1 \times 1$ cm in size was taken. After being cleaned by 0.9% saline, sample was placed on the microscope slide and then underwent MPM examination. The lesion and the surrounding normal tissue underwent MPM examination and then went through routine histopathological procedure, which included 10% buffered formalin processing, paraffin embedding, sectioning at $5 \mu\text{m}$, and then H-E staining. MPM images and H-E images were compared by an attending hepatopathologist, and then the MPM diagnostic features were established.

In the blinded study, 164 consecutive liver specimens were obtained from the liver tissue bank at the Liver Cancer Institute of Fudan University. Each specimen from the tissue bank was approximately $1 \times 0.5 \times 0.5$ cm in size. These specimens, stored at -80°C in the refrigerator, were from 164 consecutive patients who had undergone hepatectomy between September 2010 and July 2011. Specimens transported by liquid nitrogen container underwent MPM examination and then went through routine histopathological procedure.

2.3 MPM Examination

The MPM system used in this study has been described previously.²¹ The MPM system contained a high-throughput scanning inverted Axiovert 200 microscope (Zeiss LSM 510 META) and a mode-locked femtosecond Titanium: sapphire (Ti:s) laser (110 fs, 76 MHz), tunable from 700 to 980 nm (Coherent Mira 900-F). For high-resolution imaging, a high-numerical-aperture, oil immersion objective (Plan-Apochromat 63 \times , N.A.1.4, Zeiss)

was employed in MPM examination. In the multichannel mode, the backward SHG and two photon-excited fluorescence (TPEF) signals from the tissue sample were collected by the photomultiplier META detector, which had eight independent-channels and each channel could selectively be set to detect emission signals within the random range from 377 to 716 nm to achieve imaging. One channel was corresponding to the wavelength range of 387 to 409 nm to show microstructure of tissue component from SHG signals (red color-coded), whereas another channel was covered with the wavelength range from 430 to 708 nm to present the morphology of tissue component from TPEF signals (green color-coded). Moreover, to further display cell metabolism, two channels (430 to 490 nm and 500 to 560 nm) were used to collect TPEF signals from NADH and FAD of the cells. These two channels possessed the same system parameters and NADH and FAD redox ratio was shown by yellow color-coded images. The excitation wavelength λ_{ex} used in this study is 800 nm. All the images had a 12-bit pixel depth. The images were obtained at $2.56 \mu\text{s}$ per pixel.

2.4 Statistical Analysis

Currently, H-E staining is the golden standard for the diagnosis of liver cancer. We hypothesized that H-E diagnostic accuracy was 100% and MPM diagnostic accuracy was 95% in the blinded study, and then the sample size in the blinded study was 164. With this number of specimens, the study would have 90% power to detect a 5% difference between MPM diagnostic accuracy and H-E diagnosis accuracy (one-sided type I error = 0.05).

3 Results

3.1 Patient Demographics and Specimens Characteristics

There were 60 fresh liver specimens from 60 patients who had undergone hepatectomy in the pilot study, and 164 consecutive liver specimens from the liver tissue bank in the blinded study. Patient demographics and specimens characteristics were shown in Table 1.

3.2 MPM Diagnostic Features for Liver Cancer and Benign Diseases in the Pilot Study

Each of the liver specimens and surrounding normal tissue were examined by MPM. MPM images were obtained by two channels: broadband autofluorescence from cells and SHG from tissue collagen. Peak multiphoton autofluorescence intensity was detected at 800 nm.

Sixty fresh, unfixed, and unstained human liver lesions, including hepatocellular carcinomas, cholangiocarcinomas, metastatic tumors, focal nodular hyperplasias, adenomas, hemangiomas, and regenerative nodules in liver cirrhosis, underwent MPM examination and routine histopathological procedure. In the surrounding normal liver tissues, MPM images showed that the radial orientation of hepatocyte cords were around the central veins and hepatocytes were seen as one-liver-cell-thick, anastomosing, sponge-like plates, which were separated from each other by the blood-filled sinusoids [Fig. 1(a)]. These same details of cellular architecture were readily correlated with H-E images [Fig. 1(b)]. In hepatocellular carcinomas, MPM images clearly illustrated that cancer cells displayed marked cellular and nuclear pleomorphism. Cancer cells, characterized by irregular size and shape, enlarged nuclei,

Table 1 Patient demographics and tumor characteristics.

| Variable | Pilot study (N = 60) | Blinded study (N = 164) |
|--|-------------------------|----------------------------|
| Age (years), median (range) | 54 (39 to 72) | 56 (38 to 74) |
| Gender (Male/Female) | 45/15 | 131/33 |
| Body Mass Index (kg/m ²), median (range) | 24 (21 to 27) | 25 (22 to 28) |
| Tumor size (cm), median (range) | 2.0 (1.0 to 4.0) | 3.0 (1.0 to 6.0) |
| Child-Pugh score (A/B/C) | 54/6/0 | 146/18/0 |
| Histopathological diagnosis | | |
| Hepatocellular carcinoma | 26 | 93 |
| AJCC/UICC stage (I/II/III/IV) | 7/13/6/0 | 30/57/6/0 |
| Differentiation (Well/Moderately/Poorly) | 2/18/6 | 5/61/27 |
| Cholangiocarcinoma | 6 | 10 |
| Metastatic tumors | 7 | 33 |
| Colon/rectum/stomach/breast | 3/3/1/0 | 16/14/2/1 |
| Hemangiomas | 6 | 13 |
| Focal nodular hyperplasia | 6 | 8 |
| Liver adenomas | 3 | 1 |
| Regenerative nodules in liver cirrhosis | 6 | 6 |

Abbreviations: AJCC: American Joint Committee on Cancer; UICC: Union for International Cancer Control.

and increased nuclear-cytoplasmic ratio, were identified by MPM images [Fig. 1(c)], which were comparable to H-E images [Fig. 1(d)]. Moreover, in hepatocellular carcinomas, MPM imaging could significantly distinguish cancer cells from normal hepatocytes based on cell metabolism via NADH and FAD redox ratio [Fig. 1(e)], which was better in revealing cell metabolism, compared to H-E imaging [Fig. 1(f)]. The NADH and FAD redox ratio between cancer cells and normal hepatocytes was 3.11 ± 0.52 , 1.80 ± 0.24 , respectively [Fig. 1(g)]. There was significant difference ($P < 0.001$). In addition, no collagen in the intercellular space was seen in MPM imaging in hepatocellular carcinomas. Besides cell morphology and cell metabolism, tissue architecture of hepatocellular carcinomas were also seen in MPM images, which were confirmed by H-E stained images. The typical tissue architecture was trabecular or sinusoidal pattern [Figs. 2(a) and 2(b)], with exaggerated liver plates which were separated by sinusoids. The second common pattern was acinar or pseudoglandular [Figs. 2(c) and 2(d)]. Gland-like structures were formed by hepatocytes. In cholangiocarcinomas, MPM showed the clearly defined glandular and tubular structures with abundant desmoplastic stromal reaction. Dense collagenous stroma separated the glandular elements [Figs. 2(e) and 2(f)]. In liver metastatic cancers such as colorectal adenocarcinoma, MPM illustrated that normal architecture were replaced by glandular structures with cancer cells displaying marked cellular and nuclear pleomorphism [Figs. 2(g) and 2(h)]. In cavernous hemangiomas which are the most common

benign conditions, MPM showed that tumors were made up of large, cavernous vascular spaces, partly or completely filled with blood separated by scant connective tissues [Figs. 3(a) and 3(b)]. In regenerative nodules in liver cirrhosis, MPM illustrated that well-defined regenerative nodules were surrounded by vascular septa, which were typically rich in elastic fibers [Figs. 3(c) and 3(d)]. In focal nodular hyperplasias (FNH), MPM demonstrated the central, stellate fibrovascular zone, which was the most characteristic feature of FNH and has the historically entrenched name of “fibrous scar” or “scar-like fibrosis”. Hepatocytes surrounding the fibrovascular zone were arranged in incomplete nodules or pseudonodules and were partially surrounded by slender fibrous septa extending from the central fibrotic zone [Figs. 3(e) and 3(f)]. In liver cell adenomas, MPM revealed that liver lesions were composed of sheets and cords of cells arranged in two- and three-cell-thick liver plates [Figs. 3(g) and 3(h)] resembling well-differentiated hepatocellular carcinomas, but the delicate strands of collagen network alongside hepatocytes could be identified. In short, MPM images were comparable to H-E images. The MPM diagnostic features for liver cancer and benign diseases were summarized in Table 2.

3.3 MPM Diagnostic Accuracy in the Blinded Study

Using the MPM diagnostic features established in the pilot study, we performed a blinded study to evaluate the sensitivity, specificity, accuracy, positive predictive value, and negative predictive value of MPM optical diagnosis by investigating 164

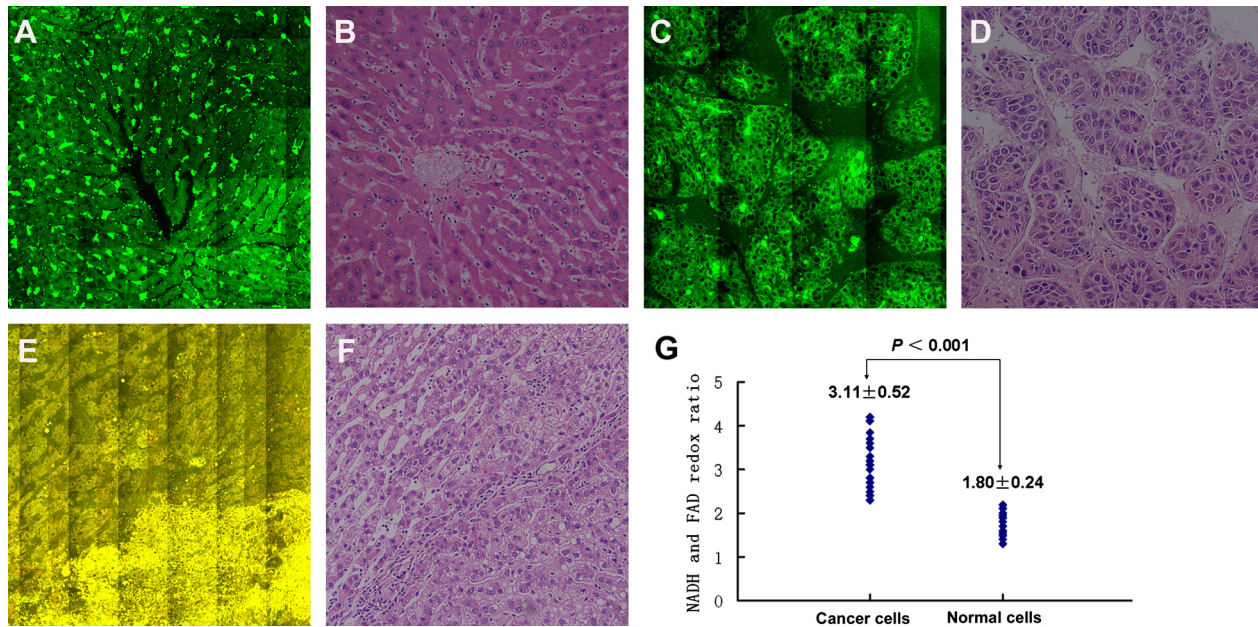


Fig. 1 Comparison of MPM images and H-E images in normal liver tissue and cancerous tissue. (a) MPM image (63×) of fresh, unfixed, and unstained normal liver tissue clearly reveals the blood-filled sinusoids and cords of hepatocytes, which is the typical arrangement of normal architecture. (b) The corresponding H-E image (20×) of fixed, stained liver tissue shows a similar arrangement of normal architecture. (c) MPM image (63×) of fresh, unfixed, and unstained cancerous tissue clearly illustrates that cancer cells display marked cellular and nuclear pleomorphism in hepatocellular carcinoma. Cancer cells were characterized by irregular size and shape, enlarged nuclei, and increased nuclear-cytoplasmic ratio. (d) The corresponding H-E image (20×) of fixed, stained cancerous tissue shows a similar cell morphology and tissue architecture in hepatocellular carcinoma. (e) MPM imaging (63×) can distinguish cancer cells (lower right) from normal hepatocytes (upper left) based on cell metabolism via NADH and FAD redox ratio in hepatocellular carcinoma. (f) The corresponding H-E image (20×) demonstrates cancer cells (lower right) and surrounding normal hepatocytes (upper left). (g) There was significantly difference in the NADH and FAD redox ratio between cancer cells and normal hepatocytes (3.11 ± 0.52 versus 1.80 ± 0.24 , $P < 0.01$).

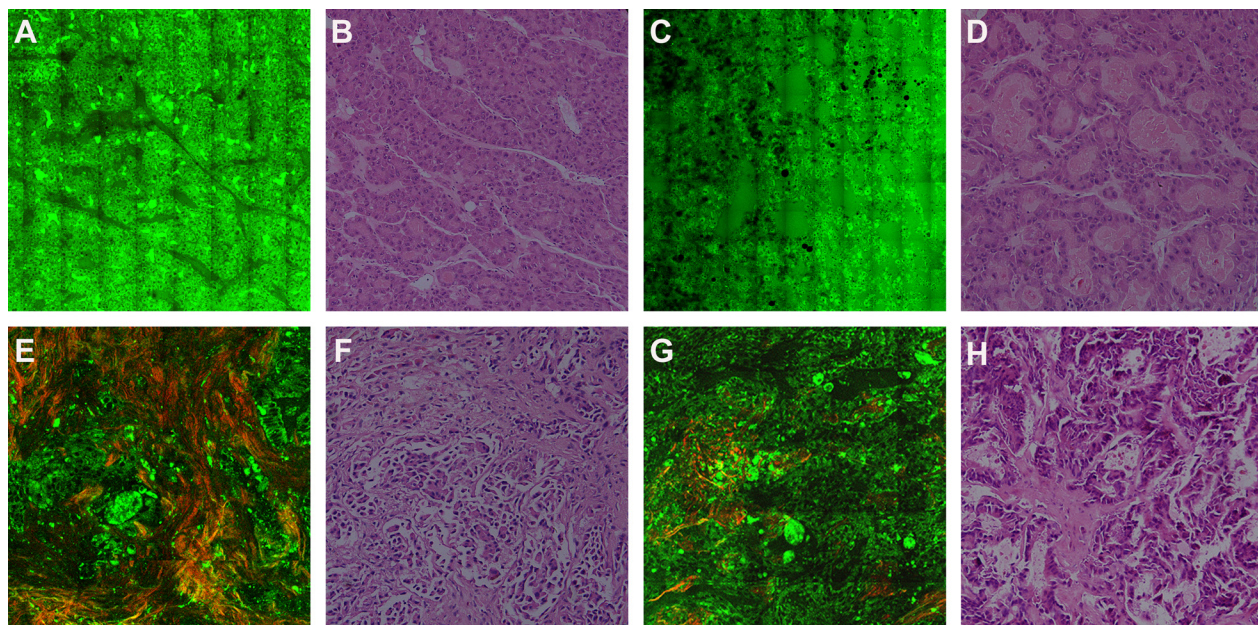


Fig. 2 Comparison of MPM images and H-E images in primary and secondary liver cancer. (a) MPM image (63×) of sinusoidal hepatocellular carcinoma. (b) The corresponding H-E image (20×) of sinusoidal hepatocellular carcinoma. (c) MPM image (63×) of pseudoglandular hepatocellular carcinoma. (d) The corresponding H-E image (20×) of pseudoglandular hepatocellular carcinoma. (e) MPM image (63×) of cholangiocarcinoma shows the glandular and tubular structures with abundant desmoplastic stromal reaction (the red color represents SHG signal, while the green color for TPEF). (f) The corresponding H-E image (20×) of cholangiocarcinoma. (g) MPM image (63×) of metastatic colonic adenocarcinoma illustrates that normal liver architecture were replaced by glandular structures with cancer cells displayed marked cellular and nuclear pleomorphism (the red color represents SHG signal, while the green color for TPEF). (h) The corresponding H-E image (20×) of metastatic colonic adenocarcinoma.

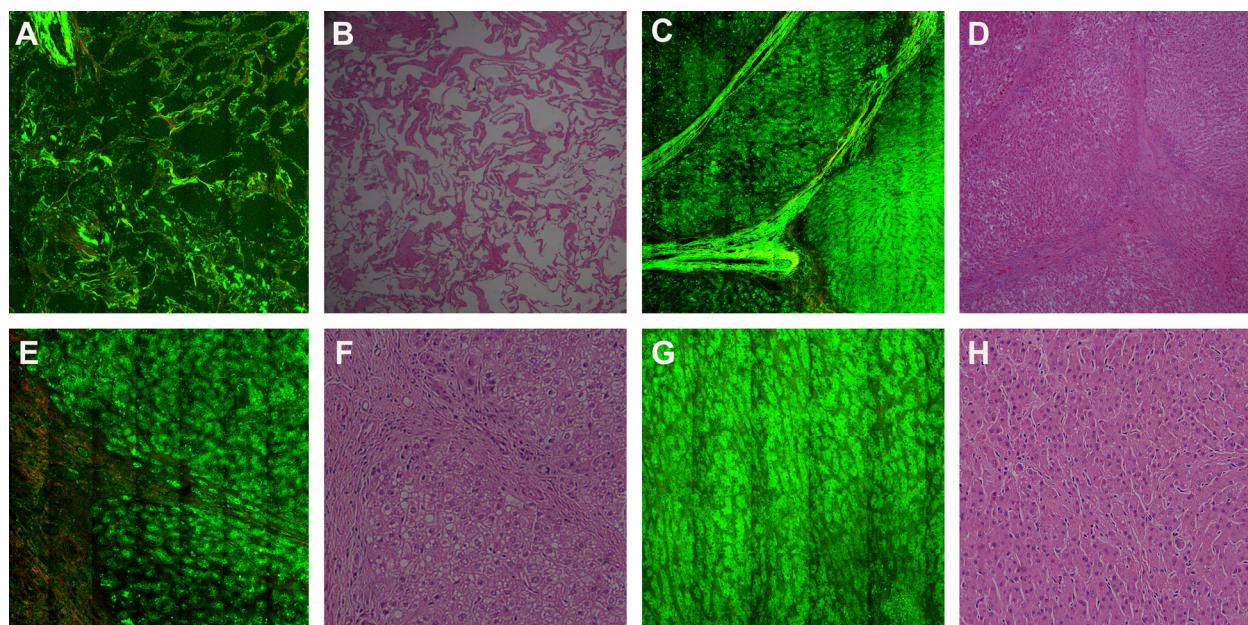


Fig. 3 Comparison of MPM images (the red color represents SHG signal, while the green color for TPEF) and H-E images in benign liver diseases. (a) MPM image (63×) of liver cavernous hemangioma shows that the tumor is made up of large, cavernous vascular spaces, partly or completely filled with blood separated by a scant connective tissue. (b) The corresponding H-E image (20×) of liver cavernous hemangioma. (c) MPM image (63×) of regenerative nodules in liver cirrhosis illustrates that well-defined regenerative nodules were surrounded by vascular septa, which were typically rich in elastic fibers. (d) The corresponding H-E image (20×) of regenerative nodules in liver cirrhosis. (e) MPM image (63×) of focal nodular hyperplasia demonstrates that stellate fibrous scar and slender fibrous septa extending to surrounding hepatocytes. (f) The corresponding H-E image (20×) of focal nodular hyperplasia. (g) MPM image (63×) of liver cell adenoma reveals that liver lesion was composed of sheets and cords of cells, arranged in two- and three-cell-thick liver plates. (h) The corresponding H-E image (20×) of liver cell adenoma.

consecutive specimens from the liver tissue bank. These specimens included primary and secondary liver cancers and benign liver conditions such as focal nodular hyperplasias, adenomas, hemangiomas, and regenerative nodules in liver cirrhosis. Both,

the attending hepatopathologist and the MPM technician, were blinded to the patient’s diagnosis. MPM images were analyzed by the attending hepatopathologist who established the MPM diagnostic features, and then the results were compared with

Table 2 MPM diagnostic features for liver cancer and benign diseases.

| Variable | Multiphoton microscopy | |
|---|---|--|
| | Two-photon-excited fluorescence | Second harmonic generation |
| Normal liver tissue | Hepatocyte cords and blood-filled sinusoids | Delicate strands of collagen network alongside hepatocytes |
| Hepatocellular carcinomas | Cellular and nuclear pleomorphism; Cancer cells with irregular size and shape, enlarged nuclei, and increased nuclear-cytoplasmic ratio; High NADH and FAD redox ratio; Thickened trabecular structures or pseudoglandular structures | No collagen in the intercellular space |
| Cholangiocarcinomas | Glandular and tubular structures with abundant desmoplastic stromal reaction | Dense collagen |
| Metastatic colorectal adenocarcinoma | Glandular structures and pleomorphic cancer cells, usually with necrosis | With or without collagen |
| Focal nodular hyperplasias | fibrous scar | Central collagen and branch |
| Liver cell adenomas | two-and three-cell-thick liver plates | Delicate strands of collagen network alongside hepatocytes |
| Cavernous hemangiomas | large, cavernous vascular spaces filled with blood | Cavernous structures of collagen |
| Regenerative nodules in liver cirrhosis | vascular septa rich in elastic fibers | Collagenous septa |

Table 3 MPM diagnostic accuracy in the blinded study.

| N = 164 | H-E diagnosis | | | |
|---------------|-------------------|-------------------------|-----------------------|-----------------------------|
| | | Cancer (N1 = 136) | Benign (N2 = 28) | |
| MPM diagnosis | Cancer (N3 = 132) | 131 | 1 | PPV = 99.24% (131/132) |
| | Benign (N4 = 32) | 5 | 27 | NPV = 84.38% (27/32) |
| | | Sens = 96.32% (131/136) | Spec = 96.43% (27/28) | A = 96.34% [(131 + 27)/164] |

Abbreviations: MPM: Multiphoton microscopy; H-E: Hematoxylin-eosin; Sens: Sensitivity; Spec: specificity; A: Accuracy; PPV: Positive predictive value; NPV: Negative predictive value.

H-E histopathology. The sensitivity, specificity, accuracy, positive predictive value, and negative predictive value of MPM in the diagnosis of liver cancer and benign diseases was 96.32% (131/136), 96.43% (27/28), 96.34% [(131 + 27)/164], 99.24% (131/132), and 84.38% (27/32) respectively. The discrepancy in MPM and H-E comparison was mainly shown in well-differentiated HCC and liver adenomas. False negative rate was 3.68% (5/136) because five cases of well-differentiated hepatocellular carcinoma were diagnosed as normal tissue, while false positive rate was 3.57% (1/28) because one sample of liver adenomas was diagnosed as well-differentiated hepatocellular carcinoma. The result of MPM diagnosis in the blinded study was shown in Table 3.

4 Discussion

4.1 Feasibility of Using MPM to Diagnose Liver Cancer

All the tumors, benign and malignant, have two basic components: (1) the parenchyma, made up of transformed or neoplastic cells, and (2) the supporting, host-derived, non-neoplastic stroma, made up of connective tissue. The parenchyma of the neoplasm determines the biologic behavior of the tumors, and it is this component from which the tumor derives its name. MPM involves the illumination of tissue by near-infrared light from a femtosecond pulsed laser, which is used to excite fluorescence from the naturally occurring fluorophores residing at the focal volume. Aside from cellular autofluorescence, MPM allows the identification of noncentrosymmetric structures such as collagen by utilizing a higher order scattering phenomenon called SHG. Using a combination of autofluorescence from cells and SHG signal from the connective tissue rich in collagen, MPM imaging can provide detailed information about tissue architecture and cell morphology. Our study showed that MPM imaging clearly demonstrated the parenchyma and the stroma in liver specimens. MPM could diagnose liver cancer and benign diseases with high sensitivity, specificity, and accuracy. These MPM images were comparable to those H-E images. Furthermore, MPM optical diagnosis has some remarkable advantages as following: (1) MPM could not only present tissue architecture and cell morphology, but also reveal cell metabolism via NADH and FAD redox ratio in live tissue without the administration of exogenous contrast agents; (2) SHG in MPM is very sensitive to collagen signal and could directly demonstrate the architecture of collagen, which was really helpful to differentiate liver cancer and regenerative nodules in liver cirrhosis patients. In addition, SHG is also good at distinguishing between liver cancer and

focal nodular hyperplasia; (3) MPM provides real-time detailed information about tissue architecture and cell morphology with high-resolution images, which can significantly save time compared to time-consuming H-E staining; (4) Real-time MPM scanning had the greater capacity for deep tissue imaging. High-resolution images could be obtained up to depths of several hundred microns in a few seconds. This advantage can be used in thick tissue imaging. In short, it is feasible to use MPM to diagnose liver cancer and differentiate benign and malignant liver lesions.

4.2 Significance of this Study

Malignant neoplasms, both primary and secondary, are common in the liver. Up to now, liver cancer in men is the fifth most frequently diagnosed cancer worldwide and the second most frequent cause of cancer-related death. In women, it is the seventh most commonly diagnosed cancer and the sixth leading cause of cancer-related death.²² Despite great improvements in diagnostic imaging procedures and serological testing, liver biopsy is still performed when the clinical behavior or the test results are not typical. However, liver biopsy has several disadvantages as mentioned above. Currently, clinical multiphoton tomography and two-photon microendoscopy provide clinicians and researchers with high resolution *in vivo* optical biopsies based on two-photon autofluorescence, SHG, and fluorescence lifetime imaging. These state of the art imaging technologies were applied in the fields of early stage melanoma detection, skin aging, nanoparticle imaging, tissue engineering, and *in situ* screening of pharmaceutical and cosmetic products. So far, more than 500 patients and volunteers in Europe, Asia, and Australia have been investigated with these novel molecular imaging tools.²⁰ The tomograph DermaInspect (JenLab GmbH, Jena, Germany) is the first *in vivo* femtosecond laser imaging system in clinical use. According to the European safety regulations, this system was safe and therefore was certified by the authorities as class 1 M device.

Since multiphoton tomography and multiphoton microendoscopy are safe in clinical use, there is an increasing demand to apply the multiphoton technology for high-resolution intrabody imaging. Our study provides the groundwork for further using multiphoton tomography and multiphoton endoscopy to diagnose liver cancer in clinic. In the short term, MPM can be used in real-time diagnosis such as intra-operative frozen section to diagnose liver cancer, judge surgical margin, and differentiate benign and malignant liver lesions. In the long term, MPM can be used in intrabody "optical biopsy" and remote consultation

with miniaturization and integration of laparoscopy. Collectively, the ultimate value of this technique would be non-destructive *in vivo* evaluation of tissue, that is, perform an “optical biopsy” of tissue by visual examination. Sub-mm-diameter probe and new photonic crystal fibers now allow fiber delivery of 100-femtosecond pulses through optical fibers with more than enough power for MPM and multiphoton endoscopy.^{15,23} All of these make it possible to allow physicians or surgeons to directly deliver high-resolution, non-invasive imaging to pathology lab, hence facilitating pathologists to make a real-time histological diagnosis immediately. This technique has the great advantage of providing results quickly in patients with liver lesions, immediately guiding the therapeutic approach such as radiofrequency ablation, ethanol injection, liver resection, or liver transplantation.

4.3 Limitation of This Study

Currently, morphology examination by histology remains the golden standard. Therefore, we performed this study to compare the morphological features between MPM imaging and H-E staining imaging. We found that MPM images were comparable to H-E images, and it was feasible to use MPM to diagnose liver cancer and differentiate benign and malignant liver lesions according to their respective morphological features. Since metabolic redox ratio is an advantage in MPM, we tested metabolic redox ratio and found the difference between cancer and normal tissue in the pilot study. However, in the blinded study, because the current golden standard of pathological diagnosis depends on morphological features and the pathologists evaluate the sensitivity, specificity, and accuracy of MPM optical diagnosis, we did not test metabolic redox ratio in the benign and malignant lesions. This is the limitation of this study. In the blinded study, the well-differentiated HCCs accounted for most of the false positive and false negative. Since usual morphology criteria are difficult to differentiate well-differentiated HCCs from some benign lesions, metabolic criteria, such as NADH and FAD redox ratio, might have important roles to solve this problem. Further investigation need to be done to confirm it.

5 Conclusions

In conclusion, it is feasible to use MPM to diagnose liver cancer and differentiate benign and malignant liver lesions. This pre-clinical study provides the groundwork for further using multiphoton endoscopy to perform real-time noninvasive “optical biopsy” for liver lesions in the near future.

Acknowledgments

This work was supported by the National Key Sci-Tech Special Project of China (2008ZX10002-025), the National Natural Science Foundation of China (30901432, 30972949, 60908043, and 30970783), the Program for Changjiang Scholars and Innovative Research Team in University (No.IRT1115), and the Natural Science Foundation of Fujian Province (2010J01136, and 2011J01341).

References

1. J. W. Marsh and I. Dvorchik, “Should we biopsy each liver mass suspicious for hepatocellular carcinoma before liver transplantation?—Yes,” *J. Hepatol.* **43**(4), 558–562 (2005).
2. M. A. Silva et al., “Needle track seeding following biopsy of liver lesions in the diagnosis of hepatocellular cancer: a systematic review and meta-analysis,” *Gut.* **57**(11), 1592–1596 (2008).
3. L. R. Rowe et al., “Subcutaneous tumor seeding following needle core biopsy of hepatocellular carcinoma,” *Diagn. Cytopathol.* **35**(11), 717–721 (2007).
4. O. M. Jones et al., “Biopsy of resectable colorectal liver metastases causes tumour dissemination and adversely affects survival after liver resection,” *Br. J. Surg.* **92**(9), 1165–1168 (2005).
5. M. Louha et al., “Liver resection and needle liver biopsy cause hematogenous dissemination of liver cells,” *Hepatology* **29**(3), 879–882 (1999).
6. W. R. Zipfel, R. M. Williams, and W. W. Webb, “Nonlinear magic: multiphoton microscopy in the biosciences,” *Nat. Biotechnol.* **21**(11), 1369–1377 (2003).
7. F. Helmchen and W. Denk, “Deep tissue two-photon microscopy,” *Nat. Methods.* **2**(12), 932–940 (2005).
8. R. Kurtz et al., “Application of multiline two-photon microscopy to functional *in vivo* imaging,” *J. Neurosci. Meth.* **151**(2), 276–286 (2006).
9. W. R. Zipfel et al., “Live tissue intrinsic emission microscopy using multiphoton-excited native fluorescence and second harmonic generation,” *Proc. Natl. Acad. Sci.* **100**(12), 7075–7080 (2003).
10. M. C. Skala et al., “*In vivo* multiphoton microscopy of NADH and FAD redox states, fluorescence lifetimes, and cellular morphology in precancerous epithelia,” *Proc. Natl. Acad. Sci.* **104**(49), 19494–19499 (2007).
11. M. Skala and N. Ramanujam, “Multiphoton redox ratio imaging for metabolic monitoring *in vivo*,” *Methods Mol. Biol.* **594**(1), 155–162 (2010).
12. F. Helmchen et al., “A miniature head-mounted two-photon microscope: high resolution brain imaging in freely moving animals,” *Neuron.* **31**(6), 903–912 (2001).
13. F. Helmchen and W. Denk, “New developments in multiphoton microscopy,” *Curr. Opin. Neurobiol.* **12**(5), 593–601 (2002).
14. S. Tang et al., “Design and implementation of fiber-based multiphoton endoscopy with microelectromechanical systems scanning,” *J. Biomed. Opt.* **14**(3), 034005 (2009).
15. H. Bao and M. Gu, “A 0.4-mm-diameter probe for nonlinear optical imaging,” *Opt. Express.* **17**(12), 10098–10104 (2009).
16. G. Liu et al., “Rotational multiphoton endoscopy with a 1 microm fiber laser system,” *Opt. Lett.* **34**(15), 2249–2251 (2009).
17. J. C. Jung and M. J. Schnitzer, “Multiphoton endoscopy,” *Opt. Lett.* **28**(11), 902–904 (2003).
18. D. Bird and M. Gu, “Two-photon fluorescence endoscopy with a micro-optic scanning head,” *Opt. Lett.* **28**(17), 1552–1554 (2003).
19. M. J. Koehler et al., “*In vivo* assessment of human skin aging by multiphoton laser scanning tomography,” *Opt. Lett.* **31**(19), 2879–2881 (2006).
20. K. König, “Clinical multiphoton tomography,” *J. Biophotonics* **1**(1), 13–23 (2008).
21. S. Zhuo et al., “Multimode nonlinear optical imaging of the dermis *in vivo* human skin based on the combination of multichannel mode and Lambda mode,” *Opt. Express.* **14**(17), 7810–7820 (2006).
22. A. Jemal et al., “Global cancer statistics,” *CA. Cancer. J. Clin.* **61**(2), 69–90 (2011).
23. D. G. Ouzounov et al., “Delivery of nanojoule femtosecond pulses through large-core microstructured fibers,” *Opt. Lett.* **27**(17), 1513–1515 (2002).